Science of the Total Environment 836 (2022) 155629

Contents lists available at ScienceDirect

Science of the Total Environment

journal homepage: www.elsevier.com/locate/scitotenv

Entropy-based Model for Gully Erosion – A combination of probabilistic and deterministic components

P.H.L. Alencar [a,b,*], A.A.F. Simplício [c], J.C. de Araújo [b]

[a] Technical University Berlin, Institut of Ecology, Ernst-Reuter-Platz 1, 10587 Berlin, Germany
[b] Federal University of Ceará, Departament of Agricultural Engineering, Campus do Pici Fortaleza, Brazil
[c] Federal Institute of Science, Technology and Education of Maranhão, Codó, Brazil

HIGHLIGHTS

- The use of Entropy Theory improves the assessment of shear stress in open channels.
- Long-term gully erosion can be modelled with few key variables for areas up to 8 ha.
- The proposed key variables are shear stress erosion and wall failure.
- Model efficiency decreases with increasing catchment areas.

GRAPHICAL ABSTRACT

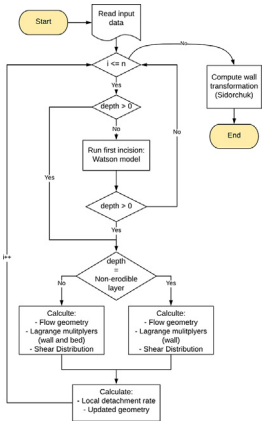

ARTICLE INFO

Editor: Manuel Esteban Lucas-Borja

Keywords:
Linear erosion
Open channel
Entropy theory
Minimum cross entropy

ABSTRACT

Gullies are a major threat to ecosystems, potentially leading to land degradation, groundwater depletion, crop loss, debris flow, and desertification. Gullies are also characterized by having a fast development and turning into primary sediment sources. Despite their impact, we have but scarce understanding of how gully erosion evolves and how to model it. In this paper, we propose a new gully erosion model that is based on the classical premise of net shear stress, i.e., hydraulic shear stress *minus* critical (resistant) shear stress, to calculate detachment rates. In order to calculate hydraulic shear stress, we developed a new equation derived from the principle of minimum cross-entropy; it was validated with laboratory measures from the literature with a Nash-Sutcliffe Efficiency of 0.95. Soil samples were analysed in the laboratory to assess critical shear stress and other soil properties. The novel gully erosion model was implemented in three gully impacted locations with catchment areas ranging from 10^{-2} to 10^{+1} ha. To assess channel geometry and eroded volumes, we used Unmanned Aerial Vehicle and Structure-from-Motion technique. The model successfully estimated long-term erosion rates, its efficiency was 0.77, and it is recommended for catchments up to 8 ha. Therefore, the new model provides planners and stakeholders with a tool to assess gully erosion, sediment yield and geometry in most areas.

1. Introduction

As far as achieving sustainable development is concerned, soil erosion has been pointed out as a central problem to be confronted in the 21st century (Borrelli et al., 2017; Poesen, 2018). Additionally, the Food and

* Corresponding author at: Technical University Berlin, Institut of Ecology, Ernst-Reuter-Platz 1, 10587 Berlin, Germany.
E-mail address: pedro.alencar@campus.tu-berlin.de (P.H.L. Alencar).

http://dx.doi.org/10.1016/j.scitotenv.2022.155629
Received 21 December 2021; Received in revised form 26 April 2022; Accepted 27 April 2022
Available online 1 May 2022

Agriculture Organization named erosion as one of the most pressing threats to soil conservation and agriculture (FAO, 2019). Soil erosion is already responsible for crop losses up to 33.7 million Mg and additional 48 km^3 of water usage yearly, affecting more severely countries like Brazil, China and India, and low-income households worldwide (Nkonya et al., 2016; Sartori et al., 2019). Among the erosion processes, gullies are critical for the functioning of hydrosedimentological processes in a catchment scale Vanwalleghem et al. (2005); Bingner et al. (2016).

Gullies are linear erosion features, that develop rapidly and are connected to land degradation, crop losses, and desertification (Valentin et al., 2005); they are, however, frequently overlooked by erosion models (Poesen et al., 2002; Poesen, 2018; Bennett and Wells, 2019). Gullies are channels carved by concentrated rainwater overflow. The runoff usually concentrates in narrow paths due to natural micro-relief (Poesen et al., 2011). This process causes an increase in sediment transport capacity, connectivity, stream power and flow shear stress, which promote the deepening of narrow channels (Valentin et al., 2005). Erosion by gully, thus increase sediment yield (Bingner et al., 2016). The resulting channels foster multiple hydrological modification at local (hillslope) and regional (catchment) scale. Locally, gullies further a reduction in groundwater storage and fertility (Valentin et al., 2005); on a catchment scale, gullies increase water and sediment connectivity from the upper areas to the outlet, causing water-body siltation and pollution (de Vente and Poesen, 2005). Due to the increase in water connectivity, gullies may also aggravate debris flow and floods (Liu et al., 2016; Wei et al., 2018).

Such considerable hydrological changes in a region have a direct impact on the economic and social activities of the respective areas. Productive lands affected by gullies present, on average, a 37% loss in agricultural production and land recuperation costs in the order of 5.2% of total expenses (Valentin et al., 2005). Gullies are impediments for human, animal and machinery movement on farmlands and may represent a risk to security of infrastructure (Alencar et al., 2020). The occurrence of gullies is usually related to changes in land use, land cover and drainage conditions, and these transformations are commonly associated with human activities such as deforestation and infrastructure development (Poesen, 2018). Gullies alone produce between 10 and 100 $Mg{\cdot}ha^{-1}{\cdot}yr^{-1}$ in affected areas, besides causing changes to water and sediment connectivities and productivity/biodiversity loss (Avni, 2005; Verstraeten et al., 2006; Poesen et al., 2011). Despite their strong impact on ecological, hydrological and social impacts (Poesen, 2018), there is a shortage of gully-erosion monitoring, as pointed by Cerdan et al. (2006), who identified a number of site-year observations of linear to be over 40 times lower than for its counterpart laminar erosion.

This process causes an increase in sediment transport capacity, connectivity, stream power and flow shear stress, which promote the deepening of narrow channels (Valentin et al., 2005). Erosion by gully, thus increase sediment yield (Bingner et al., 2016). The resulting channels foster multiple hydrological modification at local (hillslope) and regional (catchment) scale. Locally, gullies further a reduction in groundwater storage and fertility (Valentin et al., 2005); on a catchment scale, gullies increase water and sediment connectivity from the upper areas to the outlet, causing water-body siltation and pollution (de Vente and Poesen, 2005). Due to the increase in water connectivity, gullies may also aggravate debris flow and floods (Liu et al., 2016; Wei et al., 2018).

Despite their influence in hydro-sedimentological processes in a catchment scale, erosion models overlook gully erosion assessment (Poesen, 2018). Gullies are complex systems with the superposition of multiple processes, as shear stress, head-cutting, jet flow, piping, and wall failure. Therefore, gully erosion is a process with the interaction of many variables, many of which are difficult to model (Bernard et al., 2010; Castillo and Gómez, 2016; Alencar et al., 2020). Therefore, no model has ever been proposed to explain the governing forces controlling gully initiation and growing (Bennett and Wells, 2019), as gullies can vary widely in shape, scale and governing processes (Starkel, 2011).

Many models have been proposed to estimate soil loss in gullies (Thompson, 1964; Woodward, 1999; Nachtergaele et al., 2002; Wells et al., 2013; Foster and Lane, 1983; Hairsine and Rose, 1992; Sidorchuk, 1999; Dabney et al., 2015; Alencar et al., 2020). Among them, shear stress is the most used variable to describe soil detachment due to gully erosion. Nevertheless, the shear stress distribution in the boundary layer, which is decisive to assess erosive processes in channels, has not been well described mathematically.

In the Foster and Lane (1983) model (one of the most cited and used gully erosion models – Alencar et al., 2020), the soil detachment rate is directly proportional to the difference $\tau - \tau_c$. τ is the acting shear stress promoted by the discharge in the channel and τ_c the critical shear stress, a measure of soil resistance. Detachment occurs whenever $\tau \geq \tau_c$. The constant of proportionality is known as Rill Erodibility (K_r). This approach has been successfully implemented in multiple studies (Storm et al., 1990; Woodward, 1999; Casalí et al., 2003; Dabney et al., 2015), yet these net-shear-stress methods pose two challenges: (1) how to estimate soil-based parameters, i.e., critical shear stress and rill erodibility; and (2) how to estimate shear stress distribution over the channel's boundary layer (wet perimeter).

Assessing soil-based parameters such as τ_c and K_r is still an open problem (He et al., 2021). They are frequently estimated with pedotransfer functions (Alberts et al., 1989; Lal, 1994; Alberts et al., 1995). In order to assess τ_c and K_r it is common to employ percentages of sand, clay, organic matter, roots and the plasticity index; pedotransfer functions (PTF) have been implemented successfully in multiple studies (Watson and Laflen, 1986; Ascough et al., 1997; Sidorchuk, 1999; Dabney et al., 2015; Alencar et al., 2020; Luquin et al., 2021). With respect to assessing shear stress distribution on the boundary layer, several models have been proposed, such as empirical equations (Foster and Lane, 1983; Storm et al., 1990), geometric methods (Khodashenas and Paquier, 1999; Ikeda, 1982), physical-based equations (Prandtl, 1925; Smart, 1999; Yang and McCorquodale, 2004) and maximum-entropy-based equations (Chiu, 1988; Sterling and Knight, 2002; Bonakdari et al., 2014).

Linear erosion features are often classified into three groups, rills, ephemeral gullies, and classical gullies. The criteria to separate the groups, although varying among authors (Brice, 1966; Hauge, 1977; Foster et al., 1985; L, 2005), are defined by cross-section area, depth, width, flow patterns, topographic location, and nature of erosion (Douglas-Mankin et al., 2020). Rills are usually limited to very small cross-sections (< 0.01 m^2) and are not part of this study. Ephemeral gullies are usually limited to 1 m^2, typically with tillage depths and highly influenced by topography combined with anthropogenic features (e.g., crop rows and terraces). Ephemeral gullies have also the characteristic of being regularly remediated by tillage processes (Foster and Lane, 1983). Classical gullies are reported as larger than ephemeral gullies, with depths ranging from 0.5 to 30 m, steep walls and Prominent headcut (L, 2005; Douglas-Mankin et al., 2020). Classical gullies form well-defined drainage ways and often erode the entire depth of soil profile, or even soft bedrock. In this study we have channels that can be classified as ephemeral and classical gullies. However, the studied areas present long-term gullies (at least five decades) and can be classified as permanent gullies (Day et al., 2018; Alencar et al., 2020).

The objective of this paper is to propose a novel gully erosion model based on the successful net-shear-stress approach, and to validate it for a wide variety of gullies and gully-affected areas. To achieve that, we propose a new shear stress distribution equation that was derived by applying the principle of minimum cross entropy. The new shear stress distribution was validated with experimental data from literature. Subsequently, the equation was included in the EBGEM (Entropy-Based Gully Erosion Model) frame to assess net shear stress and after that, the EBGEM was validated for three gully systems of different scales.

2. Materials and methods

2.1. Entropy-based Gully Erosion Model (EBGEM)

The EBGEM is an advance with respect to the model by Alencar et al. (2020), which uses the model by Foster and Lane (1983) as the basis for a long-term modelling of small gullies with an area-based threshold parameter

to control wall geometry: cross-sections with areas above 2 m^2 have triangular or trapezoidal shape, otherwise the shape would be rectangular.

In the EBGEM, we propose applying the entropy theory to derive a novel shear stress distribution over the channel. Some of the advantages of this model are that it does not require any previous calibration (such as the threshold parameter for wall erosion) and is not limited to small gullies (drainage area up to 1 ha and depth up to 1 m), while using the same input data as the model in Alencar et al. (2020). Moreover, the EBGEM does not depend on empirical relations and the conveyance functions defined in Foster and Lane (1983). The only exception is the initial incision, which uses the Watson and Laflen (1986) equation to calculate the event-based width and depth. A complete EBGEM flowchart is presented in Fig. 1.

One of the great advances of the proposed model is the use of an accurate shear-stress distribution in the channel, which is obtained by employing the Principle of Minimum Cross-Entropy (Kullback, 1978). Appendix A extensively describes how to deduce the shear stress distribution function.

2.1.1. The principle of minimum cross-entropy (POMCE)

Kullback and Leibler (1951) first presented the concept of relative information, which was further explored in Kullback (1978). It late became known as the Kullback-Leibler Divergence (D_{KL}).

$$D_{KL}(P\|Q) = \int_{\Omega} p(x)\ ln\ \frac{p(x)}{q(x)}\,dx \tag{1}$$

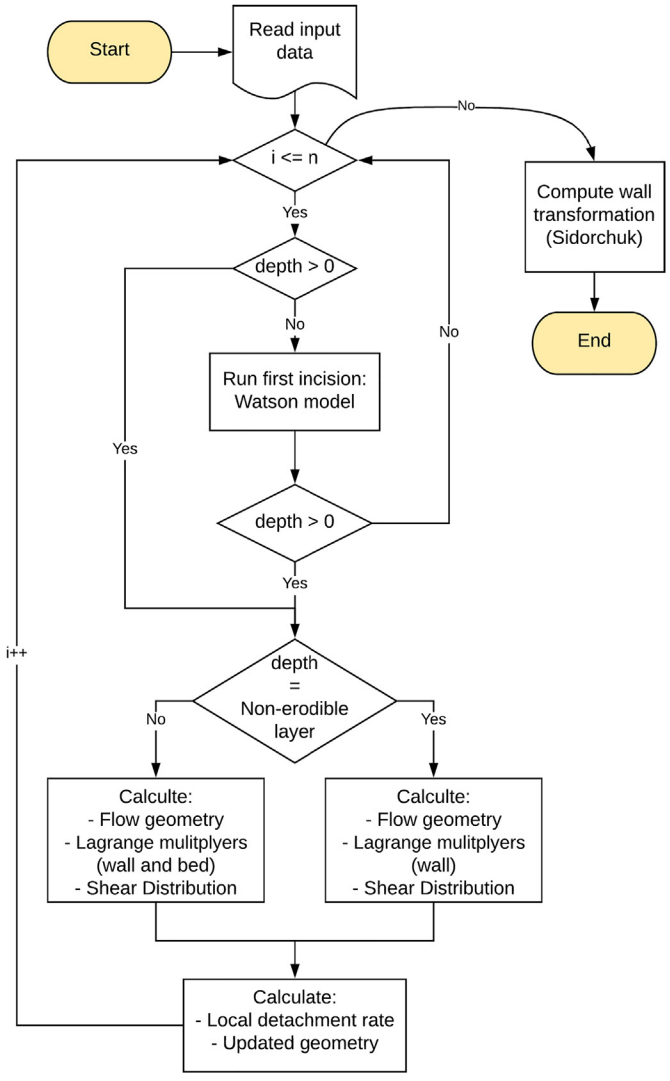

Fig. 1. Flowchart of the Entropy-Based Gully Erosion Model (EBGEM).

where P and Q are probability distributions following $p(x)$ and $q(x)$. Ω is the space (domain) of both functions.

The POMCE follows the assumption that, given a chosen function (also known as *prior* function) $q(x)$, either guessed or obtained from previous knowledge about the data, the less unbiased function $p(x)$ to represent the variable, given a set of constraints $c_i(x)$, is the one that minimizes Divergence (D_{KL}). In other words, $p(x)$ is the most similar function to *prior* $q(x)$ given the new knowledge gained by the constraints $c_i(x)$ and without assuming any unproven hypothesis.

Using the Euler-Lagrange method to solve the minimization of Eq. (1) subject to a set of constraints $c_i(x)$, one finds the Lagrangian L (Eq. (2)).

$$L = \int_{\Omega} p(x)\ ln\ \frac{p(x)}{q(x)}\,dx + \lambda_0\left[\int_{\Omega} p(x)\,dx - 1\right] + \sum_{i=1}^{n}\lambda_i\left[\int_{\Omega} c_i(x)f(x)dx - \overline{c_i(x)}\right] \tag{2}$$

where λ_0 and λ_i are Lagrange multipliers. From the method of Lagrange multipliers, one finds the following equation (Eq. (3)).

$$p(x) = q(x)\ exp\left[-1-\lambda_0-\sum_{i=1}^{n}\lambda_i c_i(x)\right] \tag{3}$$

The constraints can be expressed as functions of x and statistical moments are frequently used (Eq. (4a) and (4b)).

$$c_0(x) = \int_{\Omega} p(x)(x)dx = 1 \tag{4a}$$

$$c_1(x) = \int_{\Omega} xp(x)\,dx = \overline{x} \tag{4b}$$

Selecting a suitable *prior function* is essential for obtaining a good performance. Whenever a uniform distribution is adopted as prior function, the POMCE is reduced to the maximization of the Shannon entropy (Kumbhakar et al., 2019).

2.2. Cross-entropy shear stress equation

Using the principle of minimum cross entropy (Kumbhakar et al., 2019), we derived a novel equation to assess shear stress distribution in the boundary layer of open channels (Eq. (5); Appendix A).

$$e^{-\lambda x}(\lambda x+1) = 1-\left(1-e^{-\lambda}(\lambda+1)\right)\left(1-e^{-\lambda}(\lambda+1)\right)\frac{y}{L} \tag{5}$$

where $x = \frac{\tau}{\tau_{max}}$, y is the position over the wall or bed length (L), and λ is a Lagrange multiplier that can be obtained through the constraints (Eqs. (4a) and (4b). Also, Eqs. (16a)–(16d) in the Appendix A.1).

Eq. (5) was validated with measured data (Knight et al., 1984; Tominaga et al., 1989; Knight and Sterling, 2000) and compared with the following two equations from literature: Sterling and Knight Equation (SKE – Eq. (6); Sterling and Knight, 2002) and Ford and Labosier Equation (FLE – Eq. (7); Foster and Lane, 1983).

$$\tau = \frac{1}{\lambda}\ ln\left\{1+(\ exp\ (\lambda\tau_{max})-1)\frac{y}{L}\right\} \tag{6}$$

$$\tau = 1.35\overline{\tau}\left[1-\left(1-2\frac{X}{P}\right)^{2.9}\right] \tag{7}$$

where $\overline{\tau} = \rho gRS$. X is the distance measured from the intersection of the water surface following the wetted perimeter (P).

2.3. Experimental areas

To validate the EBGEM we surveyed three gully affected areas in Northeastern Brazil (Madalena, Gilbués and Campo Formoso – Fig. 2).

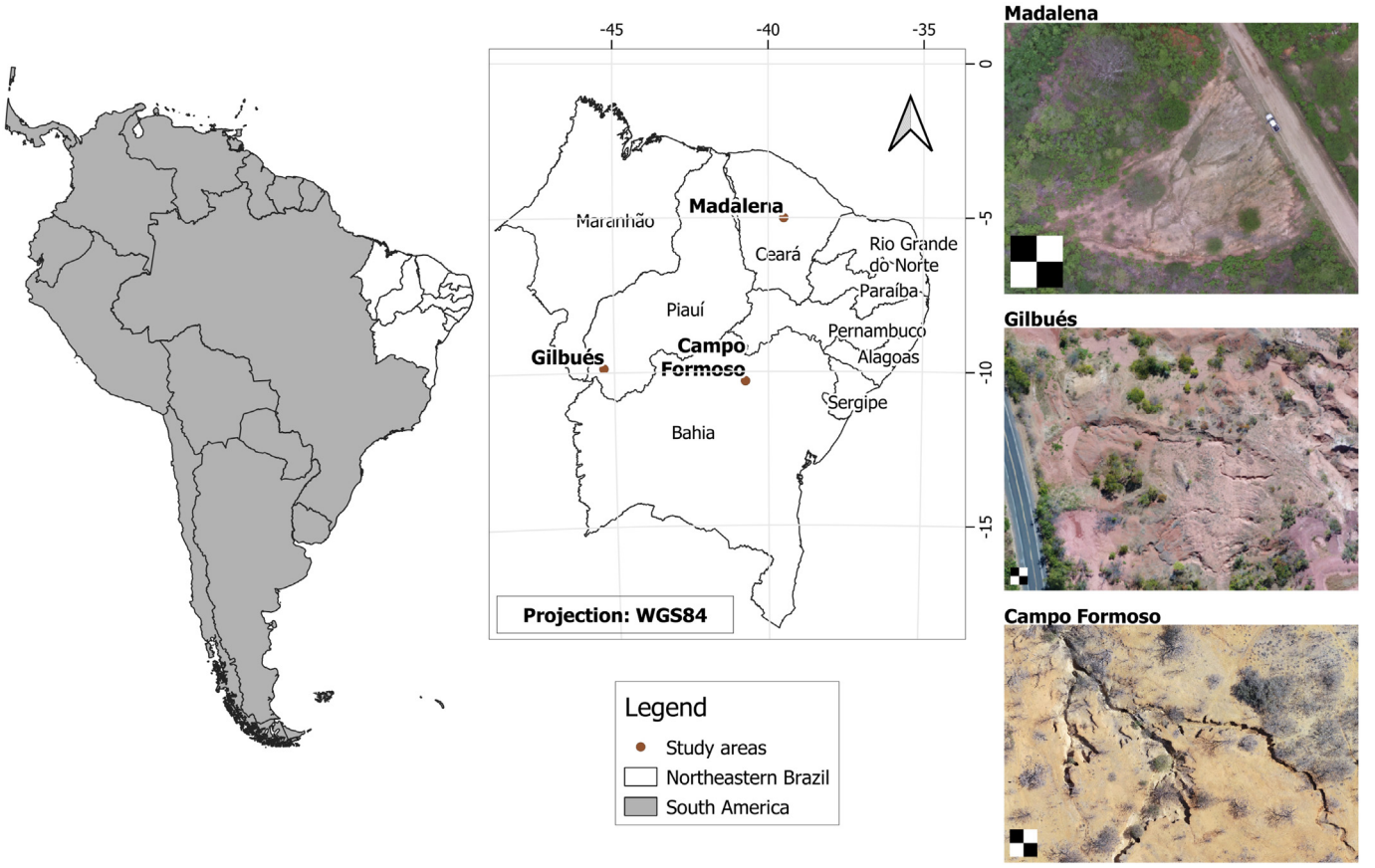

Fig. 2. Study areas in the Northeast of Brazil. On the right side, we present pictures of the landscape of each area. The scale indicated in the aerial photographs represent a 10 × 10 m square.

The Northeast of Brazil covers an area of over 10^6 km^2. Its climate is predominantly hot semi-arid (BSh, by the Köppen classification), while its vegetation mainly consists of Caatinga forest, one of the largest dry forests in the world and formed mostly by broad-leaf deciduous trees and bushes (da Silva and Rios, 2018). The average precipitation and potential evapotranspiration are 800 and 2500 mm·yr^{-1}, respectively (Pinheiro et al., 2013). Housing over 25 million people, the main activities in the region are cash-crop agriculture (sugar cane, maize, soy beans and cotton), open range cattle and fishery (Zhang et al., 2018; Coelho et al., 2017). The area is mostly situated on top of crystalline bedrock with shallow soils and limited groundwater resources (de Araújo et al., 2006). Therefore, rivers are intermittent and most water supplies rely on surface reservoirs which, due to siltation, have reduced storage capacity and water quality (de Araújo et al., 2006). This problem is aggravated by gully erosion.

The first area is located in the municipality of Madalena, State of Ceará, in the Madalena Representative Basin (MRB). The MRB houses a land reform settlement with 550 families who live from agriculture (maize, beans and vegetables), cattle raising (mainly for milk) and fishery (Coelho et al., 2017). The 75 km^2 basin has numerous gullies distributed along a road constructed in 1958 (Fig. 2). The construction of this road caused the initiation of the gully erosions due to deforestation and modification of the drainage system (Alencar et al., 2020).

The second area is located in Gilbués, State of Piauí. The Gilbués Experimental Basin (GEB) measures 6200 km^2 and is the largest desertification area in Brazil. The region has numerous badlands and gullies, some reaching dozens of meters of depth and width (Simplício et al., 2020). The main economic activities are agriculture (soy beans) and livestock.

The third area is located in Campo Formoso, State of Bahia. The Representative Basin of Campo Formoso (RBCF) stretches out over 16 ha and is also under desertification, a process that was initiated after intensive deforestation, when the native Caatinga forest was removed to produce *Agave sisalana* on the hillslopes (Jesus, 2021). *Agave* production is still the main economic activity in the region, besides livestock (da Silva and Rios, 2018).

2.4. Topography and soil survey

In the three regions, a detailed topographic survey was performed with the aid of an unmanned aerial vehicle (UAV) carrying a camera with a 16 megapixels resolution (4000 × 4000 pixels) and a field of view of 94%. Flight altitude was 50 m with frontal overlap of 80% and lateral overlap of 60%. Geo-referencing the mosaic was possible due to eight ground control points evenly distributed in each area, both in high and low ground. The coordinates of the ground control points were collected using a stationary GNSS-RTK (L1/L2) system with centimetre-level accuracy (Alencar et al., 2020).

Thanks to the application of the Structure from Motion technique (Schonberger and Frahm, 2016), it was possible to produce a detailed digital surface model (DSM) of each study area. The Structure from Motion (SfM) is founded on a three-dimensional reconstruction of the surface, it bases itself on images and the generation of a dense cloud of points obtained by matching pixels of different images and ground control points. This process results in a DSM as accurate as if obtained by through laser survey (e.g. LiDAr), while cheaper and less time-consuming (Agüera-Vega et al., 2017). The DSM pixel size (ground sample distance) ranges from two to five centimetres, while average vertical position accuracy amounts to one centimetre and average horizontal accuracy to five millimetres.

At multiple depths and locations of each study area, soil samples were extracted with an Uhland sampler. The samples were analysed in laboratory in order to investigate the physical properties of the soil which are necessary to assess critical shear stress and rill erodibility (Eqs. (8) and (9)). The detailed soil analyses results are available in the supplementary data of this paper. Table 1 presents the properties and classification of the soils

Table 1
Soil properties and classification. Each study area was subdivided according to its soil properties. The values of rill erodibility (K_r) and critical shear stress (τ_c) were calculated with Eqs. (8) and (9).

Study area	FCS[a]	VFS[b]	Silt	Clay	Organic matter	Bulk density	Soil texture[c]	Soil class[d]	K_r (s m^{-1})	τ_c (Pa)
Madalena										
Area 1	51%	19%	10%	11%	2.8%	1677	Sandy Loam	TC17	0.017	2.30
Area 2	30%	14%	17%	26%	4%	1572	Clay Loam	*Luvisol*	0.012	3.50
Gilbués										
Area 1	8%	11%	66%	16%	1.8%	1290	Silt	RQ47	0.013	3.50
Area 2	3%	26%	49%	22%	2.3%		Loam	*Neosol*	0.009	3.50
Campo Formoso										
Area 1	37%	1.2%	22%	2%	0.7%	1750	Sandy Loam	CX33 *Cambisol*	0.011	2.74
Area 2	41%	0.9%	21%	2%	0.6%				0.012	2.75
Area 3	30%	1%	36%	2%	0.6%				0.013	2.75

[a] Fine to Coarse Sand;
[b] Very Fine Sand;
[c] Soil texture classification and grain size distribution following the USDA textural classification manual (USDA, 1987).
[d] Soil class the Brazilian following the Brazilian Soil Classification System (Dos Santos et al., 2018).

in each region, following the Brazilian Soil Classification System (Dos Santos et al., 2018).

Grain size distribution was obtained using sieve analysis according to the USDA (1993). Silt and Clay fractions were obtained using the hydrometer method and organic matter (O_m) was obtained using the loss on ignition method, where dry (105 °C for 24 h) samples were set in a muffle at 400 °C for 3 h (Dos Santos et al., 2018).

Rill erodibility (K_r, in s.m.$^{-1}$) and critical shear stress (τ_c, in Pa) were estimated through pedotransfer functions (Alberts et al., 1989; Lal, 1994; Flanagan and Livingstone, 1995) that use mostly the content of sand (S_a), very fine send content (*VFS*), clay (C_l), and organic matter (O_m) (Eqs. (8) and (9)).

$$K_r = \begin{cases} 0.00197 + 0.0003 \times \mathrm{VFS} + 0.0386 \times \mathrm{e}^{-1.84\times \mathrm{O_m}} & \text{if } \mathrm{S_a} \geq 30\% \\ 0.0069 + 0.134 \times \mathrm{e}^{-0.2\times \mathrm{C_l}} & \text{if } \mathrm{S_a} < 30\% \end{cases} \quad (8)$$

$$\tau_c = \begin{cases} 2.67 + 0.065 \times \mathrm{C_l} + 0.058 \times \mathrm{VFS} & \text{if } \mathrm{S_a} \geq 30\% \\ 3.5 & \text{if } \mathrm{S_a} < 30\% \end{cases} \quad (9)$$

The variables S_a, *VFS*, C_l, and O_m are used in Eqs. (8) and (9) in percentage of mass (dimensionless).

2.5. Rainfall data

Daily rainfall data for each location throughout the whole period of analysis was provided by the Brazilian Water Agency (ANA) and the Foundation of Meteorology and Water Resources of Ceará (Funceme). Table 2 indicates the periods of analysis and rain data availability. The complete rainfall time series for all the study areas is available in the supplementary data. The rain data was tested for consistency through the double mass method, and measurement gaps (< 0.05% of the series duration) were filled with data provided by the nearest gauging station.

Since peak discharge is a measurement which is not available in any of the research areas, it was assessed using the thirty-minute maximum intensity (I_{30}) instead (Alencar et al., 2020). In order to obtain sub-daily rainfall intensity, a correlation curve between total daily precipitation and 30-min intensity was drawn (Fig. 3). This was done on the basis of data from the Experimental Basin of Aiuaba (de Figueiredo et al., 2016) with continuous monitoring of sub-daily rainfall since 2005.

Despite the average value of the coefficient of determination (R^2; Moriasi et al., 2007) in Fig. 3, a similar curve was implemented by Alencar et al. (2020). The authors argue that, although such solution can introduce uncertainty by forcing an averaged and monotonic behaviour in the relation between daily precipitation and 30-min intensity, long term analysis should minimize the effect of such uncertainties.

Table 2
Daily rainfall data availability. The start year reveals the beginning of erosion processes in all the three, coinciding with infrastructural or land use changes, e.g. road construction.

Study area	Start	End	Data source[c]
Madalena	1958	2015	Funceme[a]
Gilbués	1946	2020	ANA[b]
Campo Formoso	1967	2020	ANA[b]

[a] FUNCEME: Foundation of Meteorology and Water Resources of Ceará.
[b] ANA: National Water Management Agency.
[c] Rain gauges *Ville de Paris* (daily total precipitation).

3. Results

3.1. Cross-entropy shear stress equation

The shear stress equation (Eq. (5)) was derived by applying the Principle of Minimum Cross-Entropy, and was validated using results from 13 experiments from Knight et al. (1984), Tominaga et al. (1989), and Knight and Sterling (2000). We evaluated the gain in quality provided by the new equation when we compare t with the POME-derived equation (SKE – Sterling and Knight, 2002) and with the equation in Foster and Lane (1983, FLE). Fig. 4 exhibits the absolute error distribution of the equations compared to 181 shear stress measurements in 13 sections.

Fig. 4 conveys, a remarkable performance difference when comparing the FLE (Eq. (7)) with SKE (Eqs. (6) and (5)). The two Eqs. (5) and (6) performed very similarly, although the Cross-Entropy equation (Eq. (5)) proved to be marginally better. Multiple performance indicators for the three equations are listed in Table 3 which, at the same time, displays that Eq. (5) performed marginally better than SKE in all criteria.

3.2. Entropy-based Gully Erosion Model (EBGEM)

In this study, we measured and modelled nine gully systems from three catchments areas in the Brazilian Northeast. In total, 65 cross-sections were modelled with the EBGEM. The complete list of cross-sections and their characteristics can be found in Appendix B (Table 4). The drainage area of the gullies ranged from 10^{-3} to 10^{2} ha and channel slope from 3 to 28% (see Table 4 notes). The dimensions of carved channels also differed, with eroded area ranging from 10^{-3} to 10^{2} m^2. In Fig. 5a we show the scatter plot of measured and modelled values for all the cross-sections.

Especially in the Campo Formoso sections we can notice that the model tends to overestimate actual gully cross-section area, while no particular trend can be observed in the other catchment areas. Marker size indicates an increase in the squared error.

Fig. 5b shows the distribution of cross-section areas and assessment errors by drainage area. As expected, we observe that larger drainage areas

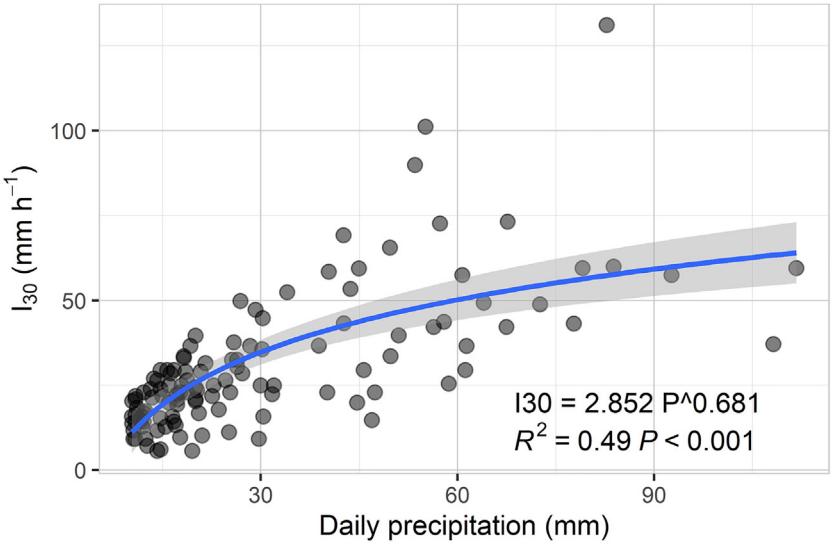

Fig. 3. Correlation between daily precipitation (P) and 30-min maximum intensity (I_{30}) at the Aiuaba Experimental Basin (de Figueiredo et al., 2016). The blue line indicates the power law regression and the shaded area the confidence interval at 95%.

produce larger cross-sections, due to higher potential of runoff accumulation and discharge. In Fig. 6 we present some model evaluators for the cross-sections. The model has an overall efficiency of 0.77 when dealing with gullies with drainage areas of up to 3 ha. When considering all the sections (with drainage area up to 16 ha), efficiency drops to 0.58.

In Fig. 6 and using the classification by Moriasi et al. (2007) we can see a good EBGEM performance in Madalena (NSE = 0.69) and Gilbués (NSE = 0.72), and an unsatisfactory one in Campo Formoso (NSE = 0.43), a locality with the largest gullies and catchment areas. This result indicates a relation between model performance and catchment area (also illustrated in Fig. 5b), which might be the key to multiple processes that are not considered in the EBGEM. Furthermore, Fig. 5 shows that the model tends to overestimate eroded area in larger sections, suggesting that processes not taken into account are protective responses to the erosion, either by human action (e.g. simple structures of sediment retention) or natural event (e.g. shielding of top layer by coarse material).

3.3. Gully growth modelling

Gully channel growth is usually described as being fast in the early stages of development, and gradually slowing down thereafter (Vanwalleghem et al., 2005; Poesen, 2018; Alencar et al., 2020). Fig. 7 shows the erosive-

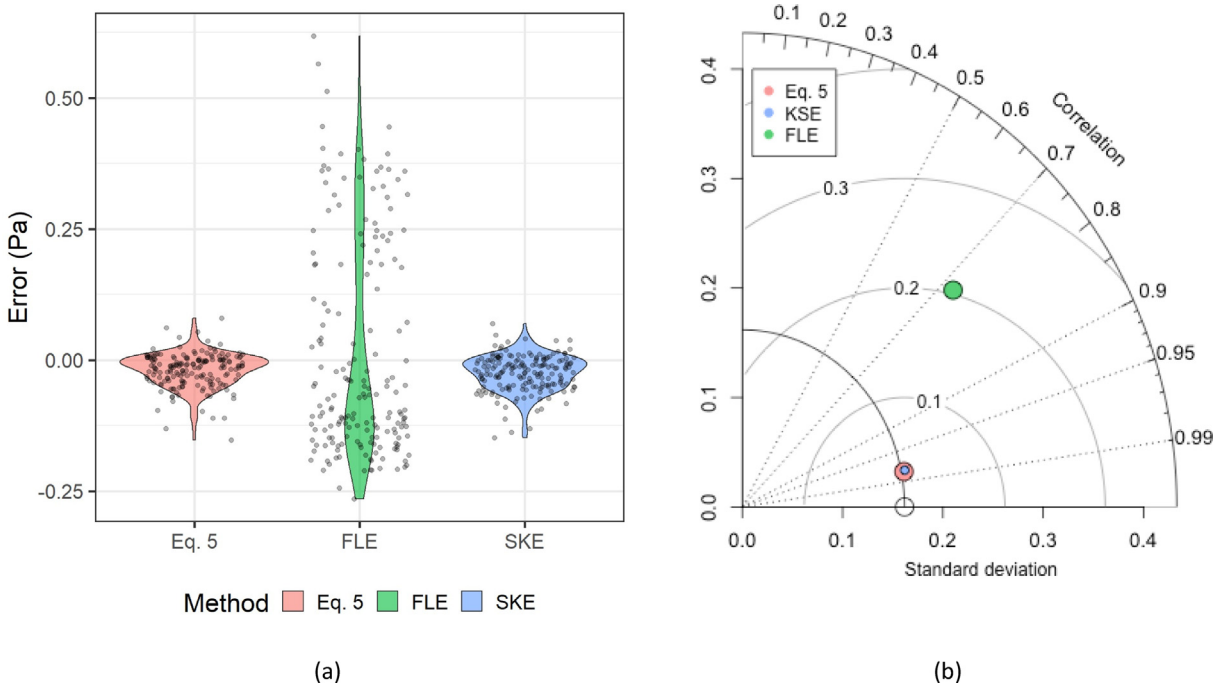

Fig. 4. (a) Absolute error distribution (violin plot - Hintze and Nelson, 1998) for the Cross-Entropy Shear Stress Equation (Eq. (5)), Foster and Lane (1983, FLE, Eq. (7)) and Sterling and Knight (2002); SKE, Eq. (6)). Black dots indicate the actual values of error for each equation. (b) The Taylor diagram presents the Pearson correlation (azimuthal angle), standard deviation of results (radial distance) and root-mean-square error (RMSE – grey contour lines) for the three equations. Note that Eq. (5) and SKE have very similar results, with Eq. (5) being marginally closer to the reference (white circle over the x-axis).

Table 3
Multiple performance indicators for the three models: EBGEM (Eq. (5)), SKE (Eq. (6)), and FLE (Eq. (7)). The modelled values were compared with experimental results (Knight et al., 1984; Tominaga et al., 1989; Knight and Sterling, 2000) of 13 cross-sections with 181 point measurements.

	Eq. (5)	SKE	FLE
NSE[a]	0.950	0.930	−0.594
RMSE[b]	0.037	0.042	0.204
PBIAS[c]	3.3%	4.3%	−2.1%
ρ_P[d]	0.981	0.979	0.728
ρ_S[e]	0.961	0.958	0.772
τ_K[f]	0.839	0.829	0.601

[a] NSE: Nash-Sutcliffe Efficiency.
[b] RMSE: Root Mean Square Error.
[c] PBIAS: Percentage of Bias.
[d] ρ_P: Pearson correlation coefficient – parametric measure of linear correlation.
[e] ρ_S: Spearman's rank correlation coefficient – non-parametric measure of rank correlation.
[f] τ_K: Kendall rank correlation coefficient – non-parametric ordinal association coefficient.

process evolution according to the EBGEM. As comparison with the model by Vanwalleghem et al. (2005) displays that the proposed model captures correctly the expected dynamic.

The equation proposed by Vanwalleghem et al. (2005; Fig. 7) has a very good agreement with measured data, presenting $R^2 = 0.97$. Nevertheless, it is interesting to note a significant deviation in the early stages ($GT < 5\%$), when most of the gullies present a faster development than the one predicted by the Vanwalleghem et al. curve. Immediately after this intense initial erosion, there is a growth deceleration relative to the Vanwalleghem et al. curve. This fact might be explained by the regime of precipitation in the Brazilian Northeast, which differs from the one of the countries where the equation was calibrated (Belgium and Russia). In our study area, precipitation tends to be convective, with 30-min intensities of up to 130 mm h^{-1} and a high inter-annual variability (Medeiros and Araújo, 2014).

4. Discussion

Soil erosion by water was pointed out as a key problem to be dealt with in order to achieve the 21st century sustainable development goals (Borrelli et al., 2017; Poesen, 2018). Gullies, as presented in Section 1 are a major threat to environments, reducing available water for vegetation and accelerating desertification processes (Valentin et al., 2005). This is particularly harmful to arid and semiarid regions, where studies on gully susceptibility mapping showed that, over 30% of the catchments in those regions have high or very high risk of gully erosion (Javidan et al., 2019; Azareh et al., 2019), potentially making gullies the main source of sediment (Bocco, 1991; Bennett and Wells, 2019). Understanding the behaviour and processes in gullies is relevant to guarantee effective actions of control and prevention (Castillo and Gómez, 2016; Bennett and Wells, 2019).

4.1. Entropy-based Gully Erosion Model (EBGEM)

The EBGEM main driver of gully erosion is shear stress, and this fact explains why the novel entropy-based shear stress distribution is so advanced. Still, gully erosion is a highly complex and non-linear process in terms of time and scale (Sidorchuk, 2005) and there are also unforeseen processes that gain relevance as the drainage area grows and, consequently, a gully system becomes more complex. In Fig. 8 we present the direct effect of a drainage area over model performance.

It can clearly been seen in Fig. 8 that, a model experiences a monotonic performance decrease when the drainage area increases. This is most likely due to the increasing complexity of gully formation in larger areas, where processes that before had apparently been negligible begin to represent important processes and influence on gully erosion. Some of such processes are, among others: shielding (Mohr et al., 2021), energy dissipation due to turbulent flow processes (Tominaga et al., 1989) and turbulent bursts (Nearing, 1991). It is interesting to highlight that the larger drainage areas in Campo Formoso have steep slopes in the head of the catchment ($S > 20\%$) and low slopes in the channel ($S < 6\%$). This leads to the erosion of coarser material from higher regions of the catchment and to its later

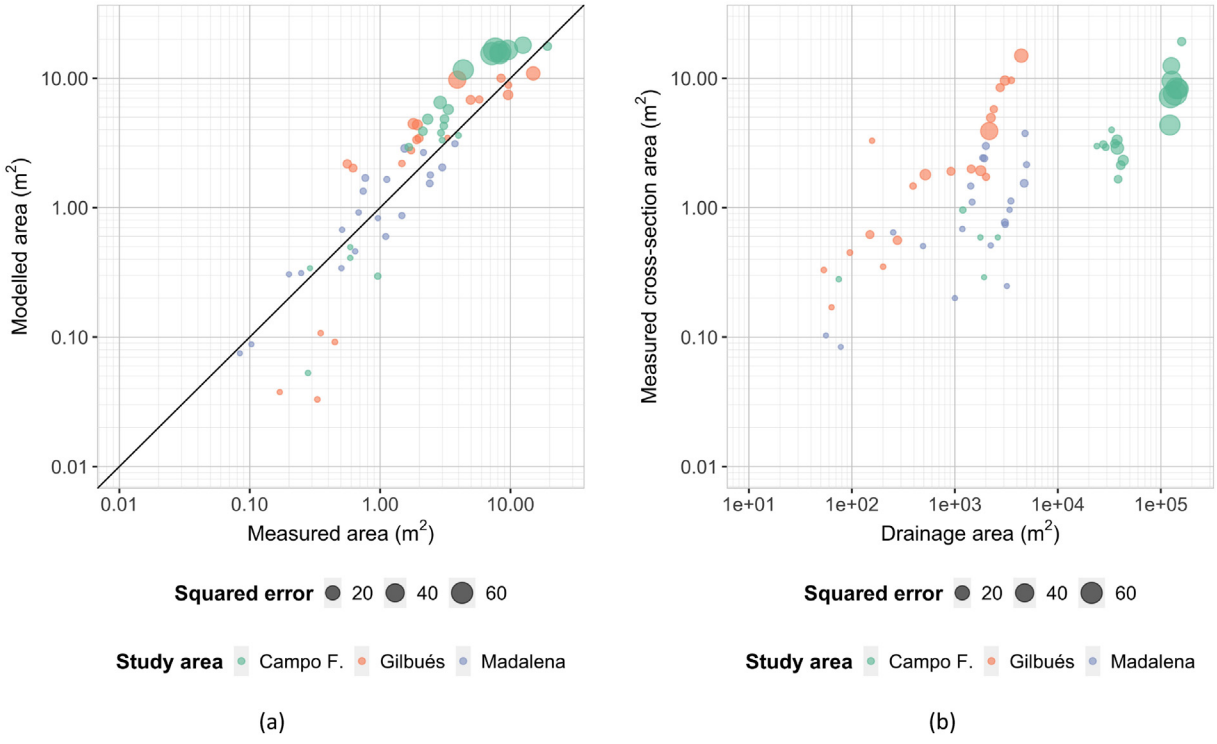

Fig. 5. (a) Measured and modelled area of the 65 modelled cross-sections in the three study areas in Brazil: Campo Formoso, Gilbués, and Madalena. (b) Drainage area versus cross-section area. The size of the markers indicate the squared error. Larger drainage areas tend to lead to larger cross-sections and larger errors.

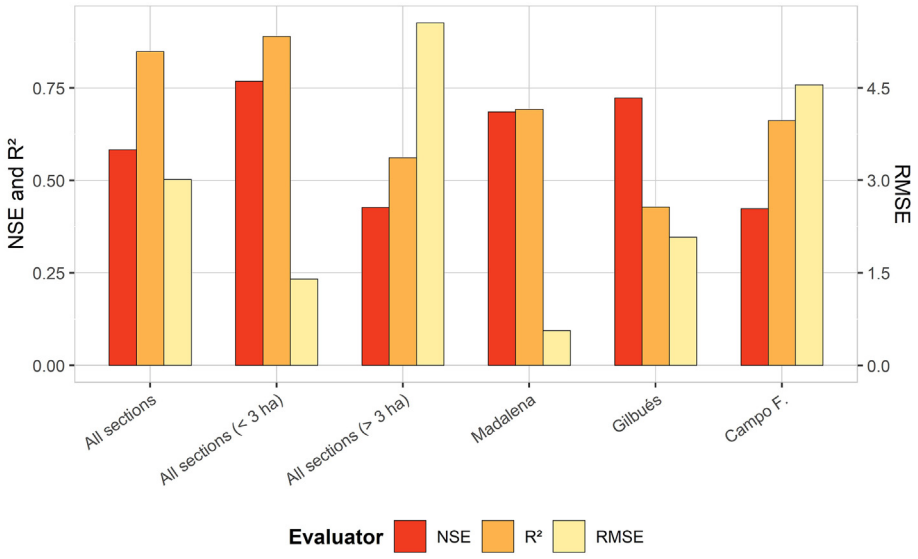

Fig. 6. Performance indicators (NSE, R^2 and RMSE) for the model and the three research areas. We also show the values for all sections and when separated by large (> 3 ha) and small (< 3 ha) drainage areas.

deposition in the channel, as observed in the field (see respective photographs in the supplementary data to this paper). The overestimation bias observed for large sections and/or drainage areas (Fig. 5) could be explained by an overestimation of the runoff and transport capacity.

In Fig. 9 we compare the results of the coupled Foster-Lane-Sidorchuk Model (Alencar et al., 2020) with those of the proposed Entropy-Based Gully Erosion Model (EBGEM). The FL-S Model is based on the Foster and Lane (1983) model, and uses its shear stress distribution (FLE - Eq. (7)) to estimate erosion. It moreover includes a routine to allow simulation of long term erosion and the Sidorchuk et al. (2003) algorithm to estimate wall-failure (Alencar et al., 2020).

We can observe in Fig. 9 that the FL-SM significantly overestimates the cross-section area for sections above 5 m^2 (usually associated with large catchments). This increasing difference in larger catchments and/or sections derive from the scope of the model itself. Alencar et al. (2020) propose the FL-SM model be employed to simulate *small permanent gullies*. The model relies on (and is highly sensitive to) an additional parameter related to the cross-section area which, for larger sections, simulates a stronger response to wall erosion. Additionally, the model based on Foster and Lane (1983) assumes that the entire section is affected by erosion when net shear stress available.

One of the improvements of the new EBGEM is that it does not depend on this particular critical area parameter. This makes the EBGEM easier to implement and suitable also for larger gully systems. Both Moriasi et al. (2007) and Ritter and Muñoz-Carpena (2013) propose a threshold of NSE = 0.65 as good/acceptable for hydrological models. Borrowing this threshold and using the results in Fig. 8 makes the EBGEM model acceptable to be implemented in catchments measuring up to 8 ha.

The identified upper limit of catchment area (8 ha) is an evidence that models that rely solely on bed and wall erosion (Foster and Lane, 1983; Storm et al., 1990; Sidorchuk, 1999; Torri and Borselli, 2003; Dabney et al., 2015; Alencar et al., 2020) are not sufficient to model more complex gully systems, that occur in larger catchments and which channels may reach dozens of meters of depth and width. In order to model such

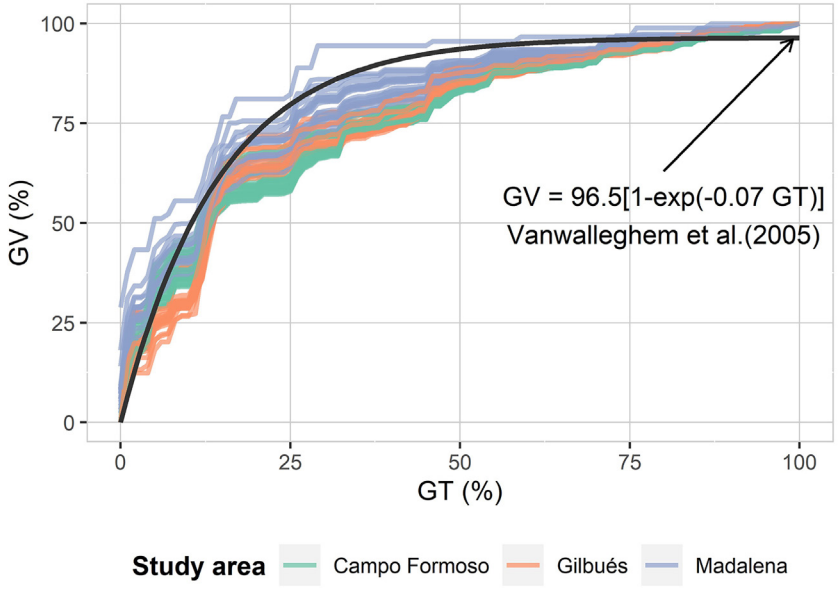

Fig. 7. Growth dynamic of all the gullies. The black continuous line represents the model proposed by Vanwalleghem et al. (2005). *GT* is the percentage of gully age (time) over the total and *GV* the percentage of gully volume over the total.

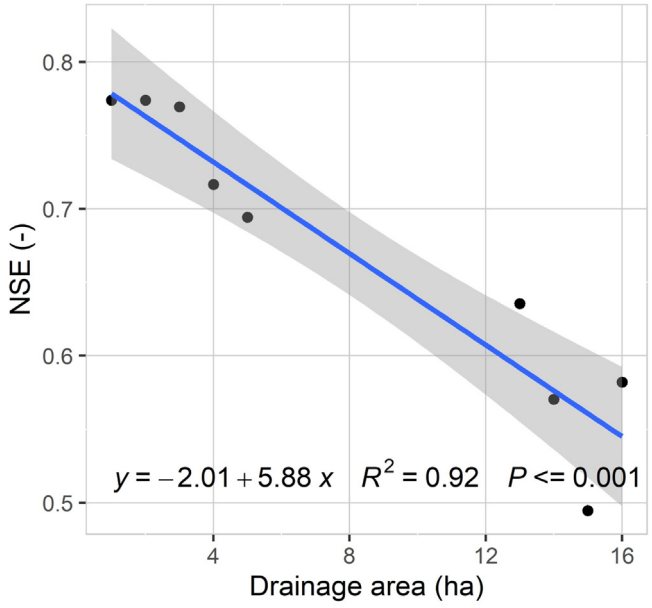

Fig. 8. Effect of drainage area on model efficiency. Each point indicates the NSE calculated for the set of gullies with drainage areas up to the value in the x-axis (e.g., for the point at 4 ha, all gullies with drainage area up to 4 ha were used to calculate NSE). The blue line stands for the linear regression between the area and the Nash-Sutcliffe efficiency coefficient (NSE), while the grey-shaded area represents the 95% confidence interval. No gullies with drainage area between 6 and 12 ha were measured.

processes, more energy and sediment inputs are required (Alonso et al., 2002; Sidorchuk, 2015; Bennett and Wells, 2019).

Nevertheless, an advantage of the EBGEM is that it is not bounded by regional features and can be easily implemented in other regions. Shear stress is based on channel geometry, differently from more conventional approaches (Storm et al., 1990; Torri and Borselli, 2003; Casalí et al., 2003). Critical shear stress and rill erodibility are estimated from pedotransfer functions obtained using Water Erosion Prediction Project (WEPP) equations (Alberts et al., 1995; Ascough et al., 1997), that were obtained from experiments in a wide range of soils. Nevertheless, when available, local values can be used. Furthermore, the limit of 8 ha established in this paper comprises most gully systems. Multiple studies that investigated the relation of catchment area and gully erosion identified that most gullies are within this limit (Vandekerckhove et al., 2000; Nachtergaele et al., 2001; Knapen and Poesen, 2010; Yibeltal et al., 2019).

Additionally, the proposed model includes a novel shear stress equation, that presents better performance than other well published approaches (Sterling and Knight, 2002; Bonakdari et al., 2014) and a shorter computational time (Bonakdari et al., 2014; Khozani and Bonakdari, 2018) is of interest not only to gully erosion modelling, but to channel engineering in general. Shear stress distribution in channel boundary layer is important also to estimate channel durability and flow resistance (Knight et al., 1994), velocity distribution (Tominaga et al., 1989), erosion and deposition (Storm et al., 1990), sediment transport (Chiu, 1988), and river morphology (Khodashenas and Paquier, 1999).

4.2. Cross-entropy shear stress equation

Entropy-based equations constitute a significant improvement compared to the empirical equation used by Foster and Lane (1983). A disadvantage of the latter is that the distribution shape never changes and that it assumes a continuous differentiable function. Such functions, however, can only be observed in a cross-section with that has a wetted perimeter following a path that is differentiable itself (e.g., circular and parabolic), as the circular sections studied by Knight et al. (1994). In rectangular, trapezoidal or any other section with vertexes, the shear stress distribution on the boundary layer presents a discontinuity (Chiu, 1988; Tominaga et al., 1989; Knight and Sterling, 2000). Eq. (5) provides a distinct parameterization for each part (edge) of the section, and this significantly improves its performance.

Eq. (5) also performed better than the maximum entropy-based equation of Sterling and Knight (2002). The Principle of Maximum Entropy (POME) is a particular case of the Principle of Minimum Cross-Entropy (POMCE), and occurs when the prior function used in POMCE is a uniform probability distribution (Kullback, 1978). By using the POMCE and a prior function that resembles more the probability distribution of shear stress values, we are able to obtain a better fitted function while maintaining the same number of unknown parameters (Lagrange multiplier λ).

Eq. (5) (RMSE = 0.033) also presented a better performance when compared to other entropy based models from the literature that improve upon the Sterling and Knight equation, such as Bonakdari et al. (2014, RMSE = 0.052) and Khozani and Bonakdari (2018, RMSE = 0.072), two models based on the Tsallis and the Renyi entropy theories, respectively. Our equation has the advantage of requiring the calibration of only one parameter (Lagrange multiplier λ) for each stretch of the wetted perimeter (bed and wall), while both Bonakdari et al. (2014) and Khozani and Bonakdari

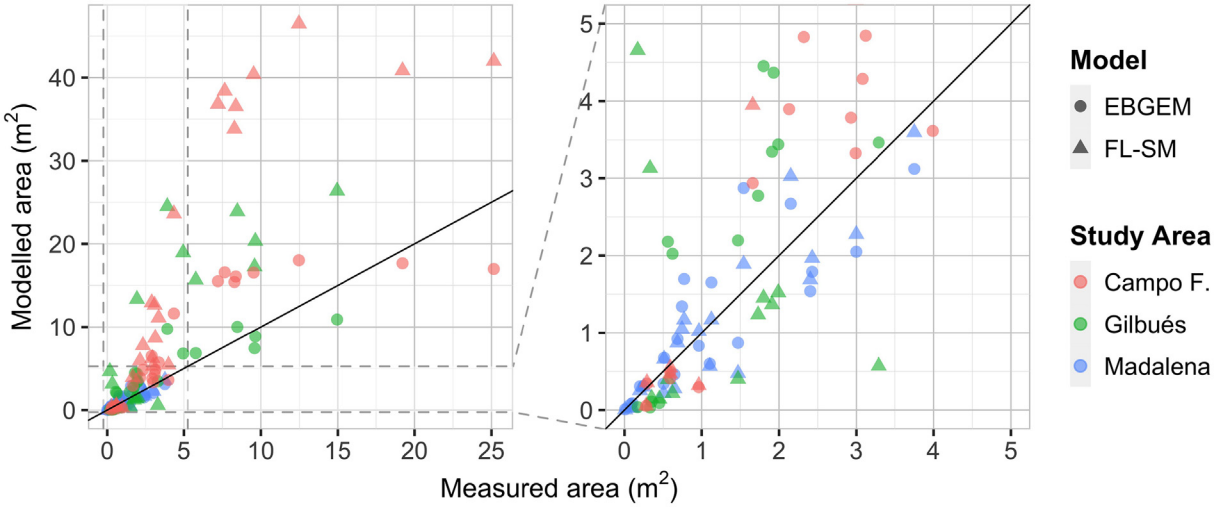

Fig. 9. Comparison between model outputs of FL-SM (Alencar et al., 2020) and EBGEM for cross-section area. The straight black line indicates the identity. It is easy to note that EBGEM results are better distributed around this line.

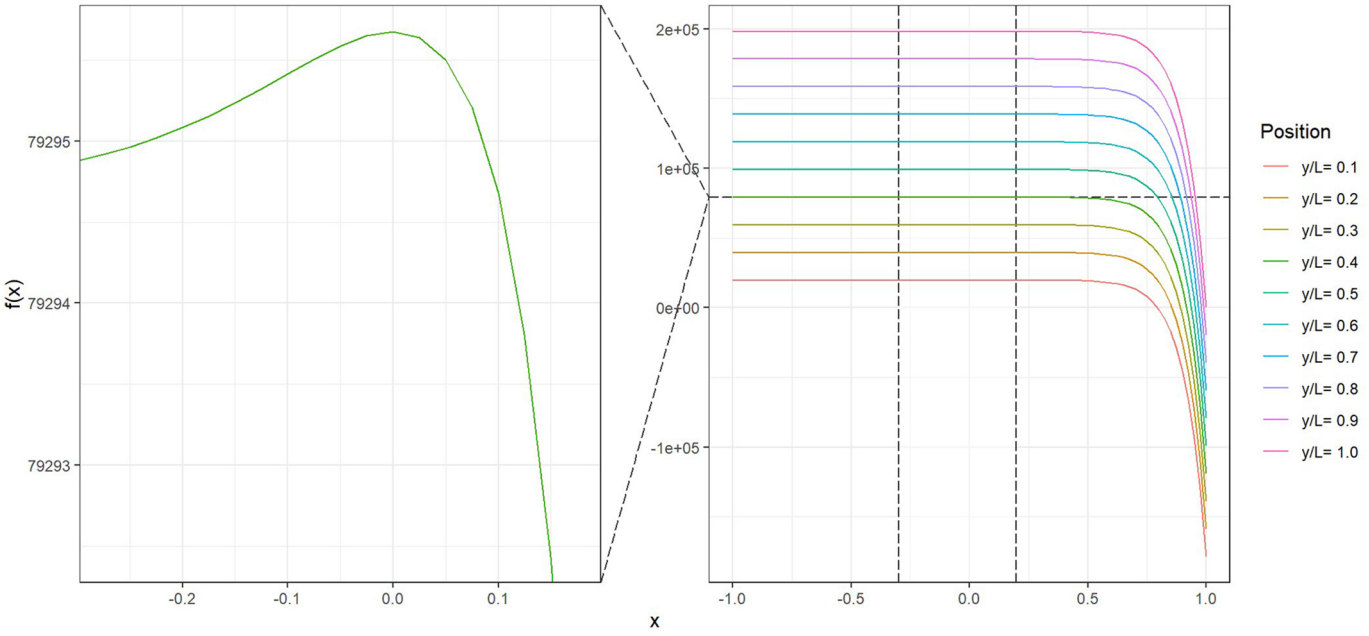

Fig. 10. Numerical example of Eq. (17a) for $\lambda = -10$.The figure illustrates the uniqueness of the solution of $f(x) = 0$.

(2018) require the calibration of two. Therefore, less computational time was needed for our equation, and this was particularly important to this study, since it was necessary to recalculate the shear stress profile at every time step.

5. Conclusions

We propose a novel gully erosion model driven by net shear stress. For the assessment of shear stress exerted by water flow, our suggestion is a novel cross-entropy-based shear stress distribution function. It is a high-performing new function in comparison to independent laboratory results, and achieves a Nash-Sutcliffe Efficiency of 0.95. The new shear stress distribution function is of interest not only for gully erosion model, but can be used in multiple fields of engineering and environmental sciences, such as sediment transport, river morphology, channel design, etc. Our new gully erosion model (EBGEM) was tested in three gully-affected areas drainage areas ranging from 10^{-2} to 10^{+1} ha, and cross-sections area ranging from 0.08 to 25 m^2. The model presented good results and attained NSE levels from 0.77 to 0.49. The drainage area plays a relevant role for model efficiency. While the model performs well for small catchments, its efficiency steadily drops for larger areas due to unforeseen processes. This is why it is recommended to implement it in catchment areas up to eight hectares, which corresponds to most of the gully systems reported in the literature. The Entropy-based Gully Erosion Model, which requires little parameterization, suits well for simulation of gullies under diverse conditions. Future outcomes should tackle additional sediment and energy sources related to gully erosion, such as head cut, pipping, and flow jets. The entropy theory has great potential to deal with uncertainties and may be used to further advance gully modelling.

Credit authorship contribution statement

PHL Alencar: Conceptualization of this study, Methodology, Programming, Field Work, Writing. **AAF Simplício:** Field Work, Image processing. **JC de Araújo:** Conceptualization of this study, Methodology, Programming, Writing.

Declaration of competing interest

The authors declare that they have no known competing financial interests or personal relationships that could have appeared to influence the work reported in this paper.

Acknowledgements

This study was partly financed by the Coordenação de Aperfeiçoamento de Pessoal de Nível Superior - Brasil (CAPES) - Finance Code 001, Capes/Print Grant 88881.311770/2018-01 and by the Edital Universal CNPq - number 407999/2016-7. Pedro Alencar is funded by the DAAD – Award Number: 91693642. Many thanks to Prof. Eva Paton for the support and advising at the Technische Universität Berlin.

Appendix A. Proof of the entropy-based shear stress equation

The Gamma distribution is very flexible and frequently used in hydrological and ecological processes (Singh, 1998). Its formulations are:

$$q(x) = Gamma(x, \alpha, \beta) = \frac{1}{\Gamma(\alpha)} \beta^{\alpha} x^{\alpha - 1} e^{-\beta x} \tag{10}$$

where α and β are parameters. By setting α and β as 2 and 1, respectively, one finds a rather simpler distribution that was used as our *prior function*.

$$q(x) = Gamma(x, 2, 1) = \gamma x e^{-x} \tag{11}$$

where γ is a scaling factor $\left(\gamma = \frac{e}{e-2}\right)$ so that $\int_0^1 q(x)dx = 1$.

We can solve Eq. (2) with the Lagrange multipliers method (Eq. (3)) and the help of selected constraints (Eqs. (4a) and (4b)).
(1) From the first constraint (Eq. (4a)) we obtain:

$$\int_0^1 \frac{e}{e-2} x e^{-x} e^{-1-\lambda_0-\lambda_1 x} dx = 1;\ \text{let}\ \frac{e^{-\lambda_0}}{e-2} = \psi\ \text{and}\ 1+\lambda_1 = \lambda \tag{12a}$$

$$\psi = \frac{\lambda^2}{1-e^{-\lambda}(\lambda+1)} \tag{12b}$$

(2) And from this first constraint (Eq. (4b)) we obtain:

$$\int_0^1 \frac{e}{e-2} x^2 e^{-x} e^{-1-\lambda_0-\lambda_1 x} dx = \overline{x} \tag{13a}$$

$$\psi \int_0^1 x^2 e^{-x(1+\lambda_1)} dx = \overline{x} \tag{13b}$$

$$\psi \left[\frac{2 - e^{-\lambda}\left((\lambda+1)^2+1\right)}{\lambda^3} \right] = \overline{x} \tag{13c}$$

From Eqs. (12b) and (13c):

$$\frac{2}{\lambda} - \frac{\lambda}{e^{\lambda}-\lambda-1} = \overline{x} \tag{14}$$

Finally, from the connection with the spatial domain:

$$\frac{1}{L}\frac{dy}{dx} = p(x) \tag{15a}$$

$$\int_0^y \frac{1}{L} dy = \int_0^x \frac{e}{e-2} x e^{-x} e^{-1-\lambda_0-\lambda_1 x} dx \tag{15b}$$

$$\frac{y}{L} = \psi \left[\frac{-e^{-\lambda x}(\lambda x+1))}{\lambda^2} \right]_0^x \tag{15c}$$

$$e^{-\lambda x}(\lambda x+1) = 1 - \left(1 - e^{-\lambda}(\lambda+1)\right)\frac{y}{L} \tag{15d}$$

Eq. (15d) cannot be further simplified, hence it becomes necessary to use numerical methods to find an explicit expression for $t(y)$.
A solution is to use the Newton-Raphson method for each y. Good approximations are expected, once the left side of Eq. (15d) grows monotonically and has a single solution.

A.1. Obtaining constraint values

Following the same premises as Sterling and Knight (2002), Knight and Sterling (2000) and Khozani and Bonakdari (2018) we assumed a division of the cross-sectional wetted perimeter in two zones (wall and bed) and also a similar behaviour of the two zones, although controlled by different parameters, yet calibrated by using the same empirical equations (6.1) of Knight et al. (1994).

$$\frac{\overline{\tau_w}}{\rho g R S} = 0.01\%SF_w \left(1 + \frac{P_b}{P_w}\right) \tag{16a}$$

$$\frac{\overline{\tau_b}}{\rho g R S} = (1 - 0.01\%SF_w)\left(1 + \frac{1}{P_b/P_w}\right) \tag{16b}$$

$$\frac{\tau_{max,w}}{\rho g R S} = 0.01\%SF_w \left[2.0372\left(\frac{P_b}{P_w}\right)^{0.7108}\right] \tag{16c}$$

$$\frac{\tau_{max,b}}{\rho g R S} = (1 - 0.01\%SF_w)\left[2.1697\left(\frac{P_b}{P_w}\right)^{-0.3287}\right] \tag{16d}$$

$$\%SF_w = C_{sf}\ exp\ (\alpha) \tag{16e}$$

$$\alpha = -3.23 log_{10}\left(\frac{P_b}{P_w C_2} + 1\right) + 4.6052 \tag{16f}$$

$$C_{sf} = \begin{cases} 1.0\ \forall\ P_b/P_w < 4.374 \\ 0.6603(P_b/P_w)^{0.28125}\ \forall\ P_b/P_w \geq 4.374 \end{cases} \tag{16g}$$

where P^b and P^w are the wetted perimeter in bed and wall, respectively; $C^2 = 1.38$. This is how we solve the Eq. (15d) for wall and bed zones.

A.2. On the validation of the unique solution of Eq. (15d)

For each $y \in [0, L]$ in Eq. (15d), let $1 - \left(1 - e^{-\lambda}(\lambda + 1)\right)\frac{y}{L}$ be equal to $-w$, where $w \in \mathbb{R}$, then:

$$f(x) = e^{-\lambda x}(\lambda x + 1)) + w = 0 \tag{17a}$$

$$\frac{df}{dx}(x) = -\lambda^2 x e^{-\lambda x} \tag{17b}$$

$$\frac{d^2f}{dx^2}(x) = \lambda^2 e^{-\lambda x}(\lambda x - 1) \tag{17c}$$

For a negative value of λ, the roots of Eq. (17b) are 0 and $-\infty$, therefore:

$$\frac{d^2f}{dx^2}(0) - \lambda^2 e^0, \text{ which is negative} \tag{18a}$$

$$\frac{d^2f}{dx^2}(-\infty) = \lambda^2 e^{+\infty}(+\infty), \text{ which is positive} \tag{18b}$$

It is also important to note that Eq. (17b), for $x \to -\infty$ is indeterminate ($-\infty \times 0$). Moreover, the roots of Eq. (17c) are $1/\lambda$ and $+\infty$. Therefore, the function has a maximum at $x = 0$ and monotonically decreases for all $x > 0$. For $x < 0$, the function reaches an asymptote at $y = w$ as $x \to -\infty$, as illustrated below.

For general cases, $\overline{x} > 0.75x_{max}$ (Foster and Lane, 1983), therefore Eq. (14) yields $\lambda < 0$. In the experimental cases, $\overline{x} \in (0.87, 0.98)$. Although physically inconsistent, it is easy to show that for $\lambda > 0$ the equations still hold with a unique solution between zero and one.

Appendix B. List of cross-sections and their characteristics

Table 4
Cross-sections and their characteristic.

Site	Gully	Sec.	DA[a]	P[b]	L[c]					Measured		Measured	
			(m^2)	(m)	(m)	K_c[d]	K_f[e]	Shape[f]	Slope[g]	A[h]	W[h]	A[h]	W[h]
Madalena	Gully 1	S1	3200	433	195	2.14	698.25	v	13%	0.25	2.26	0.31	1.98
		S2	3080	416	188	2.10	700.88	v	15%	0.74	3.19	1.34	3.41
		S3	1183	337	179	2.75	156.81	v	16%	0.68	3.56	0.92	2.82
		S4	491	108	36	1.36	265.10	t	18%	0.50	3.76	0.34	1.82
		S5	78	50	23	1.58	31.29	t	12%	0.08	1.50	0.07	1.16
		S6	3060	408	185	2.07	717.47	t	15%	0.77	2.18	1.70	3.71
	Gully 2	S1	2000	383	123	2.40	347.81	t	3%	3.00	8.93	2.05	4.14
		S2	1870	379	114	2.45	310.52	t	3%	2.43	7.32	1.79	3.89
		S3	1470	336	100	2.45	244.14	t	3%	1.11	6.89	0.60	2.62
		S4	252	80	24	1.41	126.88	t	5%	0.64	2.95	0.46	2.04
		S5	40	44	12	1.93	10.69	t	6%	0.01	0.48	0.01	0.27
		S6	1930	381	119	2.43	327.30	t	3%	2.40	7.44	1.54	3.60
		S7	1425	320	92	2.37	252.94	t	3%	1.47	6.16	0.87	2.83
	Gully 3	S1	3500	554	204	2.62	509.10	v	4%	1.13	6.32	1.65	4.19
		S2	3400	540	193	2.59	505.65	t	4%	0.96	5.54	0.83	3.39
		S3	1000	248	105	2.20	207.39	v	4%	0.20	2.18	0.31	2.05
		S4	56	49	14	1.84	16.59	t	8%	0.10	1.30	0.09	1.19
		S5	2230	473	186	2.80	283.51	v	4%	0.51	3.02	0.67	2.88
		S6	4800	620	213	2.51	764.51	v	4%	3.75	6.06	3.12	5.12
		S7	4964	639	218	2.54	769.74	t	4%	2.15	4.68	2.67	4.86
		S8	4712	609	205	2.48	763.59	v	4%	1.54	5.33	2.87	4.96
Gilbués	Gully 1	S1	2388	434	147	2.49	385.74	t	16%	5.77	6.51	6.85	7.21
		S2	2238	384	129	2.27	434.41	t	16%	4.95	5.84	6.80	7.18
		S3	2156	359	120	2.16	460.30	t	17%	3.91	3.97	9.76	8.16
		S4	1783	322	114	2.14	390.41	t	17%	1.93	2.69	4.37	6.30
		S5	1440	285	105	2.11	324.85	t	18%	1.99	2.94	3.44	6.00
		S6	916	234	83	2.16	195.91	t	20%	1.91	4.14	3.35	5.82
		S7	517	168	62	2.07	120.98	t	23%	1.80	2.68	4.45	6.07
	Gully 2	S1	277	165	68	2.77	36.07	v	8%	0.56	2.35	2.18	5.57
		S2	201	133	59	2.63	29.10	t	7%	0.35	2.17	0.11	0.34
		S3	150	160	49	3.66	11.16	v	6%	0.62	2.64	2.02	5.70
		S4	96	113	37	3.23	9.15	v	6%	0.45	2.03	0.09	0.16
		S5	64	68	22	2.40	10.99	v	6%	0.17	1.86	0.04	0.16
	Gully 3	S1	4414	407	169	1.72	1499.41	t	7%	14.95	11.68	10.90	8.64
		S2	3531	352	149	1.66	1286.78	t	7%	9.64	10.35	8.86	7.96
		S3	3065	328	139	1.66	1114.93	v	7%	9.59	9.53	7.44	7.46
		S4	2754	300	121	1.60	1078.37	v	8%	8.47	10.83	10.01	8.28
		S5	2008	97	106	0.61	5413.43	t	8%	1.73	4.61	2.77	6.52
		S6	393	261	55	3.68	28.92	v	8%	1.47	4.55	2.20	6.22

Table 4 (*continued*)

Site	Gully	Sec.	DA[a]	P[b]	L[c]					Measured		Measured	
			(m^2)	(m)	(m)	K_c[d]	K_f[e]	Shape[f]	Slope[g]	A[h]	W[h]	A[h]	W[h]
		S7	53	131	22	5.01	2.13	v	10%	0.33	3.68	0.03	0.22
		S8	157	69	29	1.53	66.74	v	24%	3.29	6.11	3.46	5.58
Campo Formoso	Gully 1	S1	27,631	1022	220	1.72	9319.94	v	7%	3.08	6.47	4.29	6.78
		S2	29,194	1037	231	1.70	10,105.06	v	7%	2.93	7.91	3.79	6.54
		S3	33,257	1103	254	1.69	11,597.34	v	6%	3.99	9.55	3.62	6.63
		S4	37,631	1189	295	1.72	12,770.22	v	6%	3.34	5.56	5.74	7.76
		S5	35,756	1144	279	1.69	12,467.05	v	6%	3.12	6.79	4.85	7.20
		S6	37,787	1196	311	1.72	12,724.11	v	6%	2.89	2.80	6.50	8.33
		S7	137,562	2891	738	2.18	28,879.38	v	7%	7.65	7.24	16.58	12.89
		S8	147,719	3024	796	2.20	30,428.23	v	6%	8.28	7.67	15.41	12.47
		S9	159,125	3169	892	2.22	32,160.02	v	6%	19.22	13.96	17.66	13.28
		S10	141,781	2912	771	2.17	30,237.01	v	7%	8.37	7.04	16.08	12.69
	Gully 2	S1	129,219	1659	665	1.29	77,391.74	t	5%	25.15	16.67	16.98	13.28
		S2	124,000	1580	610	1.26	78,562.11	t	5%	7.21	9.47	15.50	12.58
		S3	126,406	1607	650	1.27	78,959.70	t	5%	12.47	8.70	18.03	13.94
		S4	128,125	1625	630	1.27	79,343.67	t	5%	9.53	10.48	16.55	13.06
		S5	122,344	1554	590	1.24	79,047.76	v	5%	4.35	5.43	11.62	11.02
		S6	43,125	1024	448	1.38	22,609.34	v	7%	2.32	5.75	4.83	7.47
		S7	40,781	969	420	1.34	22,582.82	v	7%	2.13	5.36	3.90	7.17
		S8	38,438	918	380	1.31	22,371.65	v	7%	1.66	6.60	2.94	7.09
		S9	23,906	688	273	1.25	15,409.29	t	9%	2.99	8.55	3.33	6.21
	Gully 3	S1	1922	272	124	1.73	638.85	t	8%	0.29	3.52	0.34	2.50
		S2	2611	297	136	1.63	987.53	v	7%	0.59	5.76	0.50	2.73
		S3	1768	228	105	1.52	766.36	v	8%	0.59	3.59	0.41	2.49
		S4	1194	176	79	1.42	590.82	t	9%	0.96	6.19	0.30	2.23
		S5	75	37	14	1.21	51.25	v	10%	0.28	2.84	0.05	1.35

[a] DA: Drainage area in square metres.
[b] P: Perimeter of the drainage area in metres.
[c] L: Length of the drainage area in metres.
[d] K_g: Gravelius coefficient $\left(0.28\frac{P}{\sqrt{DA}}\right)$.
[e] K_f: Form coefficient $\left(\frac{DA}{L^2}\right)$.
[f] Shape: Indicate the general cross-section shape. "v" indicates V-shaped sections and "t" trapezoidal-shaped cross-sections.
[g] The slope refers to the local inclination of the channel. It is obtained taking the difference of height between two points in the waterpath separated by a line with length equal to 10% the length of the channel, centered in the cross-section.
[h] Area (A) and maximum width (W) of cross-sections in m^2 and m respectively.

Appendix C. Supplementary data

Supplementary data to this article can be found online at https://doi.org/10.1016/j.scitotenv.2022.155629.

References

Agüera-Vega, F., Carvajal-Ramírez, F., Martínez-Carricondo, P., 2017. Assessment of photogrammetric mapping accuracy based on variation ground control points number using unmanned aerial vehicle. Measurement 98, 221–227.

Alberts, E.E., Laflen, J.M., Rawls, W.J., Simanton, J.R., Nearing, M.A., 1989. Chapter 6: soil component. In: Nearing, M.A., Lane, L.J. (Eds.), USDA-Water Erosion Project: Hillslope Profile Model Documentation. National Soil Erosion Research Laboratory chapter 6.

Alberts, E.E., Nearing, M.A., Weltz, M.A., Risse, L.M., Pierson, F.B., Zhang, X.C., Laflen, J.M., Simanton, J.R., 1995. Soil Component. Technical Report July. USDA.

Alencar, P.H.L., de Araújo, J.C., dos Santos Teixeira, A., 2020. Physically based model for gully simulation: application to the Brazilian semiarid region. Hydrol. Earth Syst. Sci. 24, 4239–4255. https://doi.org/10.5194/hess-24-4239-2020.

Alonso, C.V., Bennett, S.J., Stein, O.R., 2002. Predicting head cut erosion and migration in concentrated flows typical of upland areas. Water Resour. Res. 38, 39-1–39-15. https://doi.org/10.1029/2001wr001173.

Ascough, J.C., Baffaut, C., Nearing, M.A., Liu, B.Y., 1997. The WEPP watershed model.1. Hydrology and erosion. Trans.ASAE 40, 921–933.

Avni, Y., 2005. Gully incision as a key factor in desertification in an arid environment, the Negev highlands, Israel. Catena 63, 185–220. https://doi.org/10.1016/j.catena.2005.06.004.

Azareh, A., Rahmati, O., Rafiei-Sardooi, E., Sankey, J.B., Lee, S., Shahabi, H., Ahmad, B.B., 2019. Modelling gully-erosion susceptibility in a semi-arid region, Iran: investigation of applicability of certainty factor and maximum entropy models. Sci.Total Environ.doi: 10.1016/j.scitotenv.2018.11.235. Sci. Total Environ. https://doi.org/10.1016/j.scitotenv.2018.11.235.

Bennett, S.J., Wells, R.R., 2019. Gully erosion processes, disciplinary fragmentation, and technological innovation. Earth Surf. Process. Landf. 44, 46–53. https://doi.org/10.1002/esp.4522 Beschuldigung.

Bernard, J., Lemunyon, J., Merkel, B., Theurer, F., Widman, N., Bingner, R., Dabney, S., Langendoen, E., Wells, R., Wilson, G., 2010. Ephemeral Gully Erosion — A National Resource Concern. U.S. Department of Agriculture NSL Technical Research Report No. 69, 67 pp.

Bingner, R.L., Wells, R.R., Momm, H.G., Rigby, J.R., Theurer, F.D., 2016. Ephemeral gully channel width and erosion simulation technology. Nat. Hazards 80, 1949–1966. https://doi.org/10.1007/s11069-015-2053-7.

Bocco, G., 1991. Gully erosion: processes and models. Prog. Phys. Geogr. 15, 392–406.

Bonakdari, H., Sheikh, Z., Tooshmalani, M., 2014. Comparison between Shannon and Tsallis entropies for prediction of shear stress distribution in open channels. Stoch. Environ. Res. Risk Assess. 29, 1–11. https://doi.org/10.1007/s00477-014-0959-3.

Borrelli, P., Robinson, D.A., Fleischer, L.R., Lugato, E., Ballabio, C., Alewell, C., Meusburger, K., Modugno, S., Schütt, B., Ferro, V., Bagarello, V., Oost, K.V., Montanarella, L., Panagos, P., 2017. An assessment of the global impact of 21st century land use change on soil erosion. Nat. Commun. 8. https://doi.org/10.1038/s41467-017-02142-7.

Brice, J.C., 1966. Erosion and Deposition in the Loess-Mantled Great Plains, Medicine Creek Drainage Basin, Nebraska Erosion and Deposition in the Loess-Mantled Great Plains, Medicine Creek Drainage Basin, Nebraska. Geological Survey Professional Paper 352 H.

Casalí, J., López, J., Giraldez, J., 2003. A process-based model for channel degradation: application to ephemeral gully erosion. Catena 50, 435–447.

Castillo, C., Gómez, J.A., 2016. A century of gully erosion research: urgency, complexity and study approaches. Earth Sci. Rev. 160, 300–319. https://doi.org/10.1016/j.earscirev.2016.07.009.

Cerdan, O., Poesen, J., Govers, G., Saby, N., Le Bissonnais, Y., Gobin, A., Vacca, A., Quinton, J., Auerswald, K., Klik, A., Kwaad, F.F.P.M., Roxo, M.J., 2006. Sheet And Rill Erosion. John Wiley & Sons Ltd., pp. 501–513 https://doi.org/10.1002/0470859202.ch38 chapter 38.

Chiu, C.L., 1988. Entropy and 2-D velocity distribution in open channels. J. Hydraul. Eng. 114, 738–756. https://doi.org/10.1061/(ASCE)0733-9429(1988)114:7(738).

Coelho, C., Heim, B., Foerster, S., Brosinsky, A., de Araújo, J.C., 2017. In situ and satellite observation of CDOM and chlorophyll-a dynamics in small water surface reservoirs in the Brazilian semiarid region. Water (Switzerland) 9. https://doi.org/10.3390/w9120913.

da Silva, A.J.P., Rios, M.L., 2018. Alerta de desertificação no médio curso do Rio Salitre, afluente do Rio São Francisco. Technical Report. IFBA, Senhor do Bonfim, Bahia.

Dabney, S.M., Vieira, D.A.N., Yoder, D.C., Langendoen, E.J., Wells, R.R., Ursic, M.E., 2015. Spatially distributed sheet, rill, and ephemeral gully erosion. J. Hydrol. Eng. 20, C4014009.

Day, S.S., Gran, K.B., Paola, C., 2018. Impacts of changing hydrology on permanent gully growth: experimental results. Hydrol. Earth Syst. Sci. 22, 3261–3273. https://doi.org/10.5194/hess-22-3261-2018.

de Araújo, J.C., Güntner, A., Bronstert, A., 2006. Loss of reservoir volume by sediment deposition and its impact on water availability in semiarid Brazil/Perte de volume de stockage en réservoirs par sédimentation et impact Sur la disponibilité en eau au Brésil semi-aride Loss of reservoir volume by se. Hydrol. Sci. J. 51, 157–170. https://doi.org/10.1623/hysj.51.1.157.

de Figueiredo, J.V., de Araújo, J.C., Medeiros, P.H.A., Costa, A.C., 2016. Runoff initiation in a preserved semiarid Caatinga small watershed, Northeastern Brazil. Hydrol. Process. 30, 2390–2400. https://doi.org/10.1002/hyp.10801.

de Vente, J., Poesen, J., 2005. Predicting soil erosion and sediment yield at the basin scale: scale issues and semi-quantitative models. Earth Sci. Rev. 71, 95–125. https://doi.org/10.1016/j.earscirev.2005.02.002.

Dos Santos, H., Jacomine, P.T., Dos Anjos, L., De Oliveira, V., Lumbreras, J., Coelho, M., De Almeida, J., de Araujo Filho, J., De Oliveira, J., Cunha, T., 2018. Brazilian Soil Classification System. Embrapa Solos-Livro técnico (INFOTECA-E).

Douglas-Mankin, K.R., Roy, S.K., Sheshukov, A.Y., Biswas, A., Gharabaghi, B., Binns, A., Rudra, R., Shrestha, N.K., Daggupati, P., 2020. A comprehensive review of ephemeral gully erosion models. Catena 195, 104901. https://doi.org/10.1016/j.catena.2020.104901.

FAO, 2019. Global Symposium on soil erosion, 15-17 May 2019, FAO, Rome. Outcome Document. URLFood and Agriculture Organization of the United Nations. http://www.fao.org/3/ca5697en/ca5697en.pdf.

Flanagan, D.C., Livingstone, S.J., 1995. Prediction Project (wepp) Version 95.7: User Summary. nserl ReportNo. 11.

Foster, G.R., Lane, L.J., 1983. Erosion by concentrated flow in farm fields. In: Simons, D.B. (Ed.), Symposium on Erosion And Sedimentation, p. 21.

Foster, G.R., Lane, L.J., Mildner, W.F., 1985. Seasonally ephemeral cropland gully erosion. Proceedings of the Natural Resources Modeling Symposium. USDA-ARS Tech. Bull, Pingree Park, CO, pp. 463–465 URL: https://www.sciencedirect.com/science/article/pii/S0378383920304993.

Hairsine, P.B., Rose, C.W., 1992. Modeling water erosion due to overland flow using physical principles: 2.Rill flow. Water Resour. Res. 28, 245–250. https://doi.org/10.1029/91WR02381.

Hauge, C., 1977. Soil erosion definitions. Calif. Geol. 30, 202–203.

He, C., Taylor, J.N., Rochfort, Q., Nguyen, D., 2021. A new portable in situ flume for measuring critical shear stress on river beds. Int. J. Sediment Res. 36, 235–242. https://doi.org/10.1016/j.ijsrc.2020.08.004 URL: https://www.sciencedirect.com/science/article/pii/S1001627920300937.

Hintze, J.L., Nelson, R.D., 1998. Violin plots: a box plot-density trace synergism. Am. Stat. 52, 181–184.

Ikeda, S., 1982. Lateral bed load transport on side slopes. J. Hydraul. Div. 108, 1369–1373.

Javidan, Kavian, Pourghasemi, Conoscenti, Jafarian, 2019. Gully erosion susceptibility mapping using multivariate adaptive regression splines—replications and sample size scenarios. Water 11, 2319. https://doi.org/10.3390/w11112319.

Jesus, D.S., 2021. Erosion in a Microbasin Under Desertification in the Middle Salitre River, Bahia. Universidade Federal do Recôncavo da Bahia – UFRB, Cruz das Almas, Brazil (in Portuguese). M.Sc. Thesis.

Khodashenas, S.R., Paquier, A., 1999. A geometrical method for computing the distribution of boundary shear stress across irregular straight open channels. J. Hydraul. Res. 37, 381–388. https://doi.org/10.1080/00221686.1999.9628254.

Khozani, Z.S., Bonakdari, H., 2018. Formulating the shear stress distribution in circular open channels based on the Renyi entropy. Phys.AStat.Mech.Applic. 490, 114–126. https://doi.org/10.1016/j.physa.2017.08.023.

Knapen, A., Poesen, J., 2010. Soil erosion resistance effects on rill and gully initiation points and dimensions. Earth Surf. Process. Landf. 35, 217–228. https://doi.org/10.1002/esp.1911.

Knight, D.W., Sterling, M., 2000. Boundary shear in circular pipes running partially full. J. Hydraul. Eng. 126, 263–275. https://doi.org/10.1061/(asce)0733-9429(2000)126:4(263).

Knight, D.W., Demetriou, J.D., Hamed, M.E., 1984. Boundary shear in smooth rectangular channels. J. Hydraul. Eng. 110, 405–422.

Knight, D., Yuen, K., Al Hamid, A., 1994. Boundary Shear Stress Distributions in Open Channel Flow. Wiley, pp. 51–88 chapter 4.

Kullback, S., 1978. Information Theory And Statistics. Dover.

Kullback, S., Leibler, R.A., 1951. On information and sufficiency. Ann. Math. Stat. 22, 79–86. https://doi.org/10.1214/aoms/1177729694.

Kumbhakar, M., Ghoshal, K., Singh, V.P., 2019. Application of relative entropy theory to streamwise velocity profile in open-channel flow: effect of prior probability distributions. Z.Angew.Math.Phys.70 https://doi.org/10.1007/s00033-019-1124-0.

L, G., 2005. A rational approach to modeling ephemeral gully erosion. REGEM: The Revised Ephemeral Gully Erosion Model. Department of Geography, State University of New York at Buffalo, U.S. Ma thesis.

Lal, R., 1994. Soil Erosion Research Methods. CRC Press.

Liu, X.L., Tang, C., Ni, H.Y., Zhao, Y., 2016. Geomorphologic analysis and a physico-dynamic characteristics of Zhatai-Gully debris flows in SW China. J. Mt. Sci. 13, 137–145.

Luquin, E., Campo-Bescós, M.A., Muñoz-Carpena, R., Bingner, R.L., Cruse, R.M., Momm, H.G., Wells, R.R., Casalí, J., 2021. Model prediction capacity of ephemeral gully evolution in conservation tillage systems. n/a. URL: https://onlinelibrary.wiley.com/doi/abs/10.1002/esp.5134Earth Surf. Process. Landf. https://doi.org/10.1002/esp.5134 arXiv: https://onlinelibrary.wiley.com/doi/pdf/10.1002/esp.5134.

Medeiros, P.H.A., Araújo, J.C.D., 2014. Temporal variability of rainfall in a semiarid environment in Brazil and its effect on sediment transport processes. J. Soils Sediments 1216–1223. https://doi.org/10.1007/s11368-013-0809-9.

Mohr, H., Draper, S., White, D.J., Cheng, L., 2021. The effect of permeability on the erosion threshold of fine-grained sediments. Coast. Eng. 163, 103813. https://doi.org/10.1016/j.coastaleng.2020.103813 URL: https://www.sciencedirect.com/science/article/pii/S0378383920304993.

Moriasi, D.N., Arnold, J.G., Van Liew, M.W., Bingner, R.L., Harmel, R.D., Veith, T.L., 2007. Model evaluation guidelines for systematic quantification of accuracy in watershed simulations. Trans. ASABE 50, 885–900 arXiv:00012351.

Nachtergaele, J., Poesen, J., Steegen, A., Takken, I., Beuselinck, L., Vandekerchove, L., Govers, G., 2001. The value of a physically based model versus an empirical approach in the prediction of ephemeral gully erosion for loess-derived soils. Geomorphology 40 (3–4), 237–252. https://doi.org/10.1016/S0169-555X(01)00046-0.

Nachtergaele, J., Poesen, J., Sidorchuk, A., Torri, D., 2002. Prediction of concentrated flow width in ephemeral gully channels. Hydrol. Process. 16, 1935–1953. https://doi.org/10.1002/hyp.392.

Nearing, M., 1991. A probabilistic model of soil detachment by shallow turbulent flow. Trans. ASAE 34, 81–0085.

Nkonya, E., Anderson, W., Kato, E., Koo, J., Mirzabaev, A., von Braun, J., Meyer, S., 2016. Global cost of land degradation. In: Nkonya, E., Mirzabaev, A., von Braun, J. (Eds.), Economics of Land Degradation And Improvement - A Global Assessment for Sustainable Development. Springer Open, Cham, pp. 117–165 https://doi.org/10.1007/978-3-319-19168-3 chapter 6.

Pinheiro, E.A.R., Costa, C.A.G., Araújo, J.C.D., 2013. Effective root depth of the Caatinga biome. Arid Environ. 89, 4.

Poesen, J., 2018. Soil erosion in the Anthropocene: research needs. Earth Surf. Process. Landf. 43, 64–84. https://doi.org/10.1002/esp.4250.

Poesen, J., Vandekerckhove, L., Nachtergaele, J., Oostwoud Wijdenes, D., Verstraeten, G., Van Wesemael, B., 2002. Gully erosion in dryland environments. Dryland Rivers: Hydrology And Geomorphology of Semi-Arid. John Wiley & Sons, Ltd., pp. 229–248 January. chapter 8.

Poesen, J.W., Torri, D.B., Van Walleghem, T., 2011. Gully erosion: procedures to adopt when modelling soil erosion in landscapes affected by gullying. Handbook of Erosion Modelling. 360–386. https://doi.org/10.1002/9781444328455.ch19.

Prandtl, L., 1925. Bericht über untersuchungen zur ausgebildeten turbulenz. Z.Angew.Math.Mech. 5, 136–139.

Ritter, A., Muñoz-Carpena, R., 2013. Performance evaluation of hydrological models: statistical significance for reducing subjectivity in goodness-of-fit assessments. J. Hydrol. 480, 33–45. https://doi.org/10.1016/j.jhydrol.2012.12.004.

Sartori, M., Philippidis, G., Ferrari, E., Borrelli, P., Lugato, E., Montanarella, L., Panagos, P., 2019. A linkage between the biophysical and the economic: assessing the global market impacts of soil erosion. Land Use Policy 86, 299–312.

Schonberger, J.L., Frahm, J.M., 2016. Structure-from-motion revisited. Proceedings of the IEEE Conference on Computer Vision and Pattern Recognition (CVPR), pp. 4104–4113.

Sidorchuk, A., 1999. Dynamic and static models of gully erosion. Catena 37, 401–414. https://doi.org/10.1016/S0341-8162(99)00029-6.

Sidorchuk, A., 2005. Stochastic components in the gully erosion modelling. Catena 63, 299–317.

Sidorchuk, A., 2015. Gully erosion in the cold environment: risks and hazards. Adv. Environ. Res. 139–192.

Sidorchuk, A., Märker, M., Moretti, S., Rodolfi, G., 2003. Gully erosion modelling and landscape response in the Mbuluzi River catchment of Swaziland. Catena 50, 507–525. https://doi.org/10.1016/S0341-8162(02)00123-6.

Simplício, A.A.F., Costa, C.A.G., Navarro-Hevia, J., Araújo, J.C., 2020. Erosion at hillslope and micro-basin scales in the Gilbués desertification region, North-Eastern Brazil. Land Degrad. Dev. https://doi.org/10.1002/ldr.3809.

Singh, V.P., 1998. Entropy-based parameter estimation in hydrology. Springer Science, Dordrecht. https://doi.org/10.1007/0-306-48065-4.

Smart, G.M., 1999. Turbulent velocity profiles and boundary shear in gravel bed rivers. J. Hydraul. Eng. 125, 106–116. https://doi.org/10.1061/(asce)0733-9429(1999)125:2(106).

Starkel, L., 2011. Paradoxes in the development of gullies. Landf.Anal. 17, 11–13.

Sterling, M., Knight, D., 2002. An attempt at using the entropy approach to predict the transverse distribution of boundary shear stress in open channel flow. Stoch.Environ.Res.Risk Assess. 16, 127–142. https://doi.org/10.1007/s00477-002-0088-2.

Storm, D.E., Barfield, B.J., Ormsbee, L.E., 1990. Hydrology and sedimentology of dynamic rill networks. Erosion Model For Dynamic Rill Networks. Vol. I. University of Kentucky, Lexington Technical Report.

Thompson, J.R., 1964. Quantitative effect of watershed variables on rate of gully-head advancement. Trans.ASAE 7, 0054–0055.

Tominaga, A., Nezu, I., Ezaki, K., Nakagawa, H., 1989. Three-dimensional turbulent structure in straight open channel flows. J. Hydraul. Res. 27, 149–173. https://doi.org/10.1080/00221688909499249.

Torri, D., Borselli, L., 2003. Equation for high-rate gully erosion. Catena 50, 449–467. https://doi.org/10.1016/S0341-8162(02)00126-1.

USDA, 1987. Soil Mechanics Level I. Module 3–USDA Textural Soil Classification. Study Guide.

USDA, 1993. Soil Survey Manual. 18. US Department of Agriculture.

Valentin, C., Poesen, J., Li, Y., 2005. Gully erosion: impacts, factors and control. Catena 63, 132–153.

Vandekerckhove, L., Poesen, J., Oostwoud Wijdenes, D., Nachtergaele, J., Kosmas, C., Roxo, M., De Figueiredo, T., 2000. Thresholds for gully initiation and sedimentation in Mediterranean Europe. Earth Surf. Process. Landf. 25, 1201–1220.

Vanwalleghem, T., Poesen, J., Nachtergaele, J., Deckers, J., Eeckhaut, M.V.D., 2005. Reconstructing rainfall and land-use conditions leading to the development of old gullies. The Holocene 15, 378–386.

Verstraeten, G., Bazzoffi, P., Lajczak, A., Rădoane, M., Rey, F., Poesen, J., De Vente, J., 2006. Reservoir and pond sedimentation in Europe. Soil Erosion in Europe. 757–774. https://doi.org/10.1002/0470859202.ch54.

Watson, D., Laflen, J., 1986. Soil strength, slope, and rainfall intensity effects on interrill erosion. Trans.ASAE 29, 0098–0102.

Wei, R., Zeng, Q., Davies, T., Yuan, G., Wang, K., Xue, X., Yin, Q., 2018. Geohazard cascade and mechanism of large debris flows in Tianmo gully, SE Tibetan Plateau and implications to hazard monitoring. Eng. Geol. 233, 172–182.

Wells, R.R., Momm, H.G., Rigby, J.R., Bennett, S.J., Bingner, R.L., Dabney, S.M., 2013. An empirical investigation of gully widening rates in upland concentrated flows. Catena 101, 114–121. https://doi.org/10.1016/j.catena.2012.10.004.

Woodward, D.E., 1999. Method to predict cropland ephemeral gully erosion. Catena 37, 393–399.

Yang, S.Q., McCorquodale, J.A., 2004. Determination of boundary shear stress and Reynolds shear stress in smooth rectangular channel flows. J. Hydraul. Eng. 130, 458–462. https://doi.org/10.1061/(asce)0733-9429(2004)130:5(458).

Yibeltal, M., Tsunekawa, A., Haregeweyn, N., Adgo, E., Meshesha, D.T., Aklog, D., Masunaga, T., Tsubo, M., Billi, P., Vanmaercke, M., Ebabu, K., Dessie, M., Sultan, D., Liyew, M., 2019. Analysis of long-term gully dynamics in different agro-ecology settings. Catena 179, 160–174. https://doi.org/10.1016/j.catena.2019.04.013.

Zhang, S., Foerster, S., Medeiros, P., Carlos, J., Araújo, D., Waske, B., 2018. Effective water surface mapping in macrophyte-covered reservoirs in NE Brazil based on TerraSAR-X time series. Int. J. Appl. Earth Obs. Geoinf. 69, 41–55. https://doi.org/10.1016/j.jag.2018.02.014.